Structural properties of $Pb(Mg_{1/3}Nb_{2/3})_{0.90}Ti_{0.10}O_3$ films deposited by pulsed laser ablation on titanium nitride substrates

A. Fundora[a,c], E. Martínez[b], O. Blanco[b], and J.M. Siqueiros[a]
[a]*Centro de Ciencias de la Materia Condensada, UNAM, Ensenada, B. Cfa., México.*
[b]*Centro de Investigación en Materiales, DIP-CUCEI, Universidad de Guadalajara, Apartado Postal 2-638, 44281, Guadalajara, Jalisco, México.*
[c]*Facultad de Física-IMRE, Universidad de La Habana, La Habana, CUBA.*

Recibido el 19 de septiembre de 2007; aceptado el 29 de noviembre de 2007

Pulsed laser ablation is used to deposit $Pb(Mg_{1/3}Nb_{2/3})_{0.90}Ti_{0.10}O_3$ (PMNT) polycrystalline thin films on TiN bottom electrodes, which in turn are prepared by DC sputtering on Si wafers. The PMNT perovskite phase formation is confirmed by x-ray diffraction analysis. The morphology of the films is analyzed by scanning electron microscopy. The nature of the ferroelectric layer-electrode interface is studied by transmission electron microscopy. The effect of the characteristics of the interface in the performance of the multilayer system is also studied. The characteristics of the TiN films, used as electrodes, are evaluated using Auger electron spectroscopy and x-ray photoelectron spectroscopy. Finally, a model for the PMNT/TiN/SiO_2/Si film system thus obtained is proposed.

Keywords: Ferroelectric thin films; PMNT; pulsed laser ablation; titanium nitride.

Se depositan películas policristalinas de $Pb(Mg_{1/3}Nb_{2/3})_{0.90}Ti_{0.10}O_3$ (PMNT) por la técnica de ablación por láser pulsado sobre electrodos de TiN que, a su vez, son crecidas por erosión iónica en DC sobre sustratos de Si. La formación de la fase perovskita del PMNT es confirmada por análisis de difracción de rayos X. La morfología de las películas es analizada por microscopía electrónica de barrido. La naturaleza de la interfaz entre la capa ferroeléctrica y el electrodo es estudiada por microscopía electrónica de transmisión. Así mismo, se estudian los efectos de las propiedades de dicha interfaz en el desempeño del sistema de multicapas. Las características de las películas de TiN, usadas como electrodos, son evaluadas mediante espectroscopía de electrones Auger y espectroscopía de fotoelectrones de rayos X. Finalmente, se propone un modelo para el sistema PMNT/TiN/SiO_2/Si de películas delgadas aquí descrito.

Descriptores: Películas delgadas ferroeléctricas; PMNT; ablación por láser pulsado; nitruro de titanio.

PACS: 77.84.-s; 68.65.Ac; 81.15.Fg

1. Introduction

Thin layer dielectric and ferroelectric ceramics have recently received attention for possible applications in microelectronic circuitry, including Ferroelectric Random Access Memory (FRAM) and Dynamic RAM (DRAM) elements and capacitors [1-3]. In terms of materials, lead magnesium niobate (PMN), lead titanate (PT), and the solid solution series $Pb[(Mg_{1/3}Nb_{2/3})_{1-x}Ti_x]O_3$ (PMNT) provide a particularly versatile choice. For example,

(i) high dielectric constant (PMN rich) thin layers are suitable for DRAM applications or

(ii) large spontaneous polarization (PT rich) are convenient for FRAM applications. Additions of PT increase the Curie temperature (T_c) and spontaneous polarization (P_s) [4].

The room temperature dielectric constant reaches a maximum value at x=0.1 [5]. The giant electromechanical strain found in this system has also made this material highly attractive for transducer and actuator applications. A direct application for high performance actuating materials is found in micro-electromechanical systems (MEMS) and with continuing trends in miniaturization, interest in MEMS has evolved to the current development of nanoelectromechanical systems[6,7].

To date, several thin film deposition techniques have been employed to produce PMNT films, including pulsed laser deposition [8-12], sol-gel [13,14], metal organic chemical vapor deposition [15] and ion sputtering deposition [16]. In order to optimize the piezoelectric properties of the films, it has been necessary to produce highly oriented and single phase samples.

The processing of PMNT films with the desired perovskite structure presents two considerable challenges:

i) the lowering of the formation temperature of the PMNT, which is regularly of the order of 800°C, too high for Si integrated technology and

ii) the obtainment of PMNT films free of the pyrochlore phase, which is thermodynamically more stable than PMNT and is promoted by lead deficiency.

McKinstry's group at Penn State obtained epitaxial PMNT films for the first time by PLD. The epitaxial effect of the substrate during film growth was insufficient to prevent pyrochlore formation, which was possible only at temperatures higher than 700°C and oxygen pressures approaching 1 Torr [17]. In particular when using the PLD technique, to optimize lead content and to eliminate the pyrochlore phase formation, the following is recommended:

i) using PbO rich targets,

ii adjusting the deposition rate through the laser repetition rate, and

iii using a high oxygen pressure atmosphere to reduce Pb loss [17].

Associated with ferroelectric thin film research is the quest for adequate bottom electrodes for ferroelectric devices. So far, the most popular materials for bottom electrodes are platinum and metal oxides such as RuO_2, $SrRuO_3$, $La_{0.5}Sr_{0.5}CoO_3$ (LSCO), where the perovskite structure of the ferroelectric materials forms at temperatures above 700°C, too high for Si integrated technology. A diffusion barrier between the electrode and the silicon wafer is one of the key issues for the integration of PMNT capacitors. This barrier is usually required to prevent the electrodes and dielectrics from reacting with Si atoms, which diffuse from the poly-Si plug during the PMNT deposition and post-deposition process. T.H. Teng *et al.* have shown good results using TiN as a diffusion barrier with BST films [18].

The present work concerns the processing and properties of $Pb(Mg_{1/3}Nb_{2/3})_{0.90}Ti_{0.10}O_3$ films for integrated capacitors deposited on titanium nitride. For the first time, titanium nitride (TiN) films deposited by RF sputtering as bottom electrodes for ferroelectric PMNT films deposited by PLD from lead rich PMNT targets are reported. TiN is a good diffusion barrier and will not participate in the oxygen chemistry at the ferroelectric-electrode interface, has good adhesion to Si and $SiO_2$and has a resistivity in the 20-100 $\mu\Omega$cm range, making it a sufficiently good conductive electrode. Fatigue, aging, and high leakage currents are the most common problems associated with these kinds of electrodes.

2. Experimental procedure

The conventional ceramic method was used to prepare the $Pb(Mg_{1/3}Nb_{2/3})_{0.90}Ti_{0.10}O_3$ target. The columbite precursor technique with excess magnesium oxide [19] was used to prevent the formation of pyrochlore phases [20] that depress the dielectric properties of lead oxide based ferroelectric ceramics [21]. The samples were prepared with high purity reagents (E. Merck, Darmstadt, Germany). MgO powders with 5% excess and Nb_2O_5 were prefired at 1000°C for 4 hours with a 1°C/min heating rate to form the $MgNb_2O_6$columbite structure. The powders were ground in an agate mortar and mixed with PbO and TiO_2, prefired at 800°C for 2 hrs and finally sintered into 22 mm diameter disks at 1200°C for 2 hrs with a heating rate of 1°C/min.

TiN films to be used as bottom electrodes were grown on SiO_2/Si(100) wafers by using reactive sputtering of titanium in a 9 to 1 mixture of argon and nitrogen at a pressure of 0.6 Pa, with a substrate temperature of 450°C. The PMNT films were deposited using Pulsed Laser Deposition (PLD) in a high vacuum chamber with a base pressure of 10^{-4} Pa. Both the target and the substrate were fixed in rotating mounts, moving at a constant angular speed to favor thickness uniformity. A KrF excimer laser (LEXTRA 200 by Lambda Physik) with a 248 nm wavelength, 30 ns pulse duration, 10Hz repetition rate and 2 J/cm^2 fluence was used for the target ablation. The distance between the target and the TiN/SiO_2/Si (100) substrate was 100 mm. For the deposit, at an oxygen pressure of 26 Pa, the substrate was initially heated to 250°C and maintained at that temperature for a few tens of pulses, in order to provide the deposited material with enough mobility to form a continuous layer. The heat supply was then turned off and the rest of the deposit took place as the substrate cooled down to room temperature. The resulting films were annealed at 500, 550 and 600°C (named hereafter PMNT500, PMNT550 and PMNT600, respectively) at ambient pressure for 15 sec. Ruthenium films were deposited as top electrodes by DC sputtering of a ruthenium target in an argon atmosphere of 0.14 Pa at room temperature. Depth profiles of Ru/PMNT/TiN/SiO_2/Si films were performed in a Scanning Auger Microprobe (SAM) PHI-595 equipped with a differentially pumped Ar^+ ion gun. The crystal orientation of the films was determined by XRD using the Cu Kα_1 (λ_1= 1.54056 Å) and Kα_2 (λ_2 =1.54439 Å) lines of an XRD Phillips X'Pert-MPD diffractometer with a scanning rate of 2°/min.

X-ray photoelectron spectroscopy (XPS) analysis was performed in a Perkin-Elmer PHI 560/ESCA-SAM system, equipped with a double-pass cylindrical mirror analyzer and a base pressure of 10^{-8}Pa. Argon ion sputtering was performed with 4keV energy and 0.36 μA/cm^2 current beams, yielding an average sputtering rate of 3 nm/min. All XPS spectra were obtained before and after 10 min of Ar^+ sputtering. For the XPS analyses, samples were excited with 1486.6eV energy $Al_{K\alpha}$ x-rays. XPS spectra were obtained under two different conditions:

(i) a survey spectrum mode with a normal resolution of 1.5eV and

(ii) high, 0.4eV resolution.

Binding energy calibration was based on C 1s at 284.6eV. The surface morphology of the PMNT films was examined with a JSM-5300 JEOL scanning electron microscope (SEM). Cross-sections of the samples were examined with a JEOL 2010 transmission electron microscope (TEM). Selected area diffraction (SAD) and micro-diffraction were used to determine the crystalline phases present.

3. Results and discussion

3.1. XRD and SEM results

Figure 1a shows the XRD pattern of the PMNT500. A perovskite polycrystalline phase is observed in this case, where the peaks from the silicon substrate and TiN electrode are indicated. Apparently no pyrochlore residual secondary phase

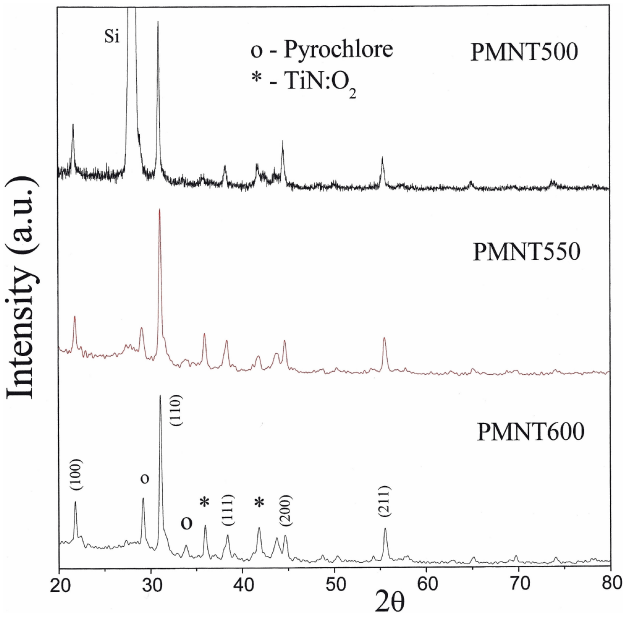

FIGURE 1. X-ray diffraction patterns of the PMNT ferroelectric thin films deposited by Pulsed Laser Ablation at 250°C and postannealed at 500°C (PMNT500), 550°C (PMNT550) and 600°C (PMNT600).

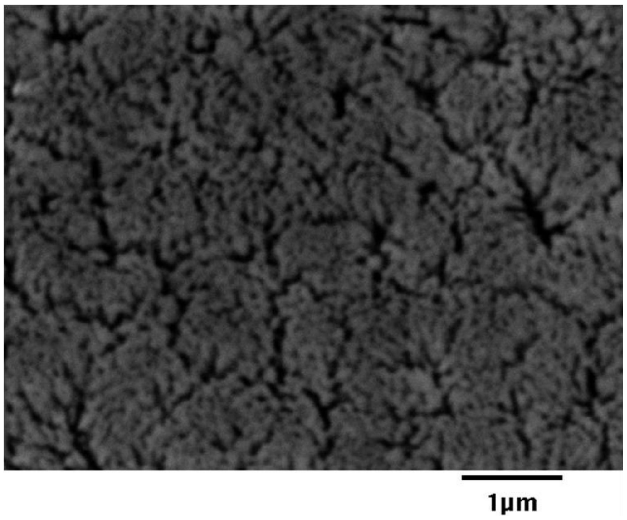

FIGURE 2. SEM micrograph of a PMNT ferroelectric thin film deposited on TiN:O_2 and postannealed at 550°C.

is present. This result shows the formation of the PMNT system on a TiN layer with a perovskite crystal structure at a lower temperature (500°C) than previously reported by other deposition techniques [9,21,23]. Figures 1b and 1c also show the XRD patterns of the PMNT550 and PMNT600 samples respectively, where a polyphasic polycrystalline growth is observed. A residual pyrochlore phase is now present, growing as the annealing temperature is increased. However, the perovskite phase is clearly the dominant crystalline phase. The reason for the pyrochlore formation as the temperature increases is that above 500°C the solid solution becomes lead deficient due to lead volatilization, allowing the formation of a pyrochlore phase isostructural with the $Pb_2Nb_2O_7$-type pyrochlore phase [24,25]. Deterioration of the dielectric properties of the film is to be expected for higher annealing temperatures. A significant fraction of the species supplied by the laser-generated plume will thus condense as Pb^{2+}- ion containing clusters, which are probably amorphous, for a period long enough that the Pb^{2+}revaporizes from the noncrystalline phase of the films [22]. These films are, therefore, more likely to lose Pb^{2+}- ions, and then Pb^{2+}- deficient secondary phases will be more easily formed.

Figure 2 shows an SEM micrograph of the PMNT550 thin films. Similar microstructure was obtained for the PMNT500 and PMNT600 samples, where granular growth was not observed in any case within the resolution of our instrument. Grain boundaries are clearly defined and represent a considerable fraction of the film material. It is to be expected that they would play an important role in the dielectric behavior and transport properties of the samples. Cracking of the PMNT films is expected, due to the difference in thermal expansion coefficients between the film and the substrate. Such cracks develop in the post-annealing process, which is performed at a higher temperature than that of the deposit. Nevertheless, the higher the deposit temperature, the higher the Pb^{2+} vaporization. This is the reason why the deposition temperature must be relatively low and post-annealing is needed. Short circuits between the top and bottom electrodes due to Ru paths percolating along the cracks were not detected by resistivity measurements. To determine how deep the top electrode material penetrates into the films, Auger Electron Spectroscopy (AES) was performed on the samples.

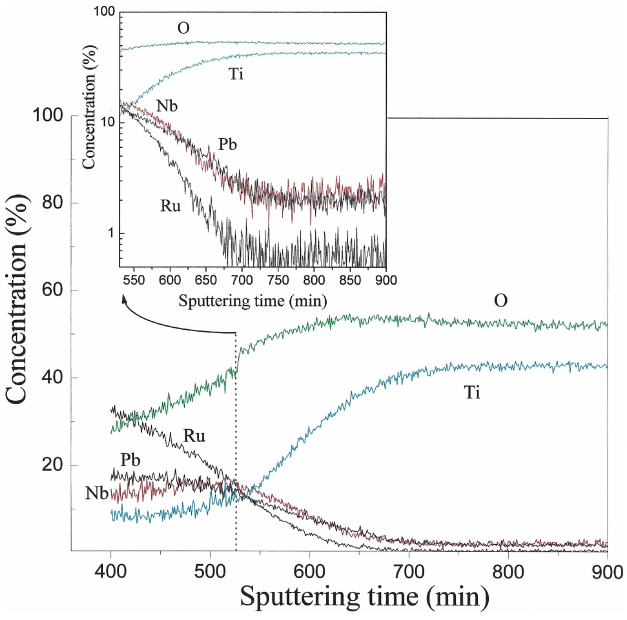

FIGURE 3. Concentration profile of the component elements of the Ru/PMNT600/TiN:O_2/Si thin films obtained by Auger Electron Spectroscopy.

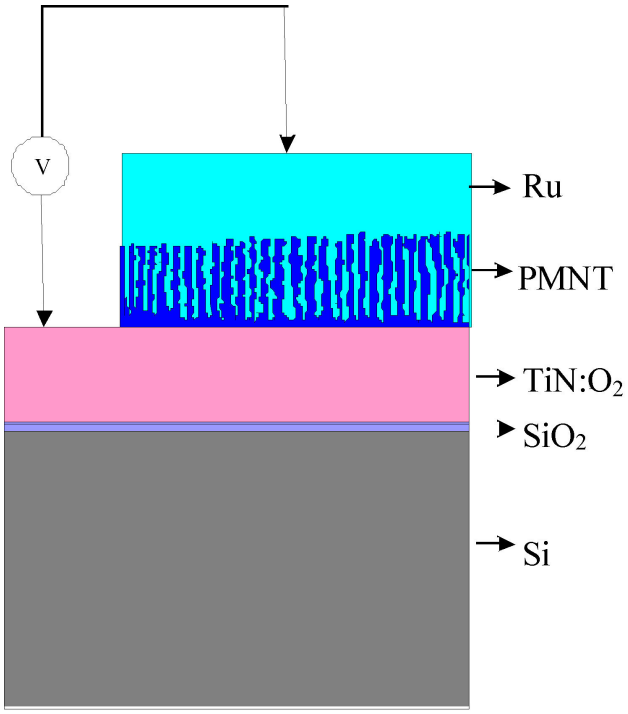

FIGURE 4. Model for the interfaces in the Ru/PMNT/TiN:O_2/Si system, suggested by the SEM and AES results presented in Figs. 2 and 3, respectively.

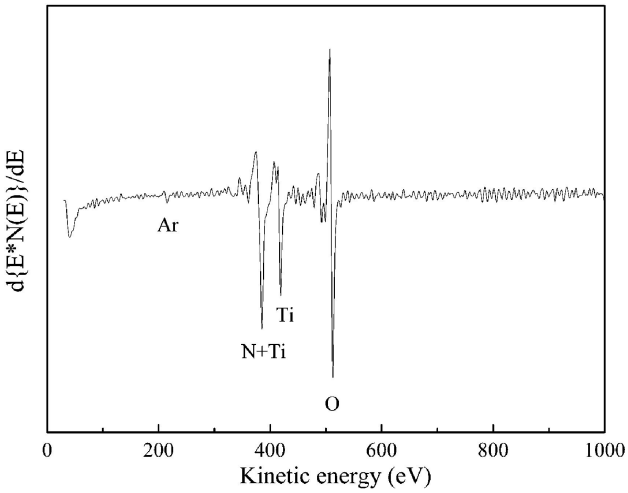

FIGURE 5. AES spectrum of the TiN electrode region, in the crater sputtered off by an Ar-ion beam of the PMNT600 sample.

3.2. AES and XPS spectroscopy analysis

A depth profile study was done on the PMNT600 sample to study the film composition along its thickness from the surface to the substrate. A concentration profile against sputtering time of the component elements of the sample made in real time is presented in Fig. 3. There is no sharp interface between the layers of the system because ruthenium is found coexisting with the components of the PMNT film, although no percolation of metallic ruthenium was found by resistance measurements. The interface between PMNT and TiN must be diffuse as a result of long sputtering times. The TiN-Si interface is better defined, and only silicon and oxygen from the silicon natural oxide are detected in the center of the crater. The presence of Ru in the PMNT films suggests either a diffusion process of the Ru into the PMNT films or intercolumnar Ru deposited between neighboring columns of the PMNT films. Electrical measurements ruled out the first possibility since the PMNT films were not conducting. The second possibility leads us to propose the model presented in Fig. 4, requiring transmission electron microscopy (TEM) studies for confirmation.

The Auger spectrum of the TiN region in the crater is shown in Fig. 5, where the presence of oxygen is continuously detected as the electron beam travels from the PMNT film through the TiN layer. The oxygen concentration, peak shape and position, suggest an oxidation of the TiN film, forming an oxi-nitride [23] compound by reacting with residual oxygen in the deposit chamber. The reason the oxygen peak appears much higher than the nitrogen peak in the spectrum, indicating higher oxygen concentration, is probably due to the high level of oxidation of the electrode surface during the deposit of the ferroelectric material, performed at a high temperature in the presence of ambient oxygen or by the ambient atmosphere after the deposit [26]. In the Auger measurements, the peaks assigned to elementary titanium and nitrogen overlap, making the nitrogen to oxygen concentration ratio in the electrode very difficult to evaluate. That is why, in order to measure the nitrogen/oxygen ratio in the bottom electrodes, XPS measurements had to be taken at the surface as well as inside the electrode film in a TiN film before the PMNT deposit.

In Fig. 6, the XPS spectra for the TiN electrode is shown to analyze its surface and bulk oxidation state.

Figure 6a shows the XPS survey spectrum of the as-deposited surface of the TiN film. The XPS analysis shows that the O 1s (531eV), Ti $3p_{3/2}$ (457eV), N 1s (396eV), C 1s (284eV) and Si $2p_{1/2}$ (101eV) core level principal peaks are present. Figure 6b is a high-resolution spectrum in the 452-464eV interval obtained after a previous Argon ion erosion to get to the bottom of the TiN electrode. This spectrum shows the Ti $2p_{3/2}$ and Ti $2p_{1/2}$ peaks, where the overlap between different peaks associated with different bonds of the titanium cation can be seen. The Ti $2p_{3/2}$ peak located at 458eV is due to titanium atoms bound to oxygen as TiO_2 [27], while the Ti $2p_{3/2}$ peak located at 454.8eV is due to titanium atoms bound to nitrogen corresponding to TiN. On the surface of the film before the erosion process, the signal component associated with TiO_2 is higher than that of TiN because of the oxidation of the surface after the TiN deposit. However, after erosion, the peak associated with the TiN bond becomes more intense; this confirms that the oxygen source is associated with the PMNT deposition performed at a high temperature in the presence of ambient oxygen.

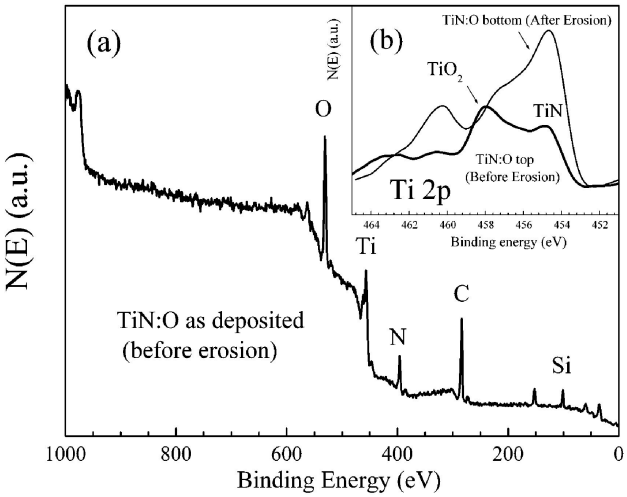

FIGURE 6. a) XPS spectrum of an as-deposited TiN film (before PMNT deposition) used as a bottom electrode and b) high resolution XPS analysis of the titanium compound.

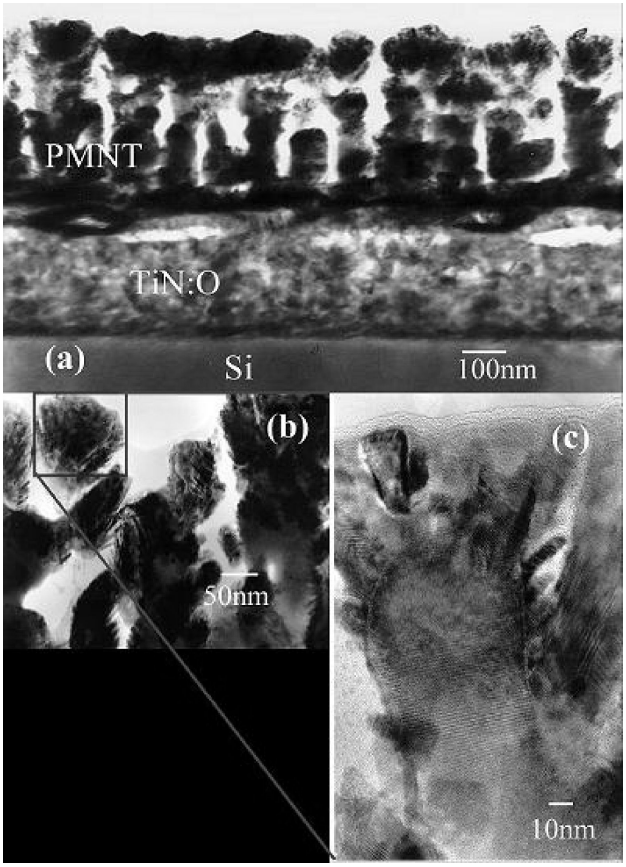

FIGURE 7. a) Cross-section TEM micrograph of the PMNT/TiN:O_2/Si thin film postannealed at 600°C (PMNT600), b) TEM micrograph making evident the granular structure of the film and c) high resolution TEM micrograph, where coupling between the crystalline planes of different grains is observed.

3.3. Cross-section TEM results

The reason for studying the cross-section of the films is to evaluate the electrode-ferroelectric film interface characteristics and the effect of the growth habit of the ferroelectric film [29] on the dielectric properties of the system. It is well known that the degradation mechanisms suffered by the ferroelectric films are attributable, in many cases, to an amorphous layer formed between the ferroelectric film and the electrode [30]. From the AES results, where a pyrochlore phase between the perovskite phase and the bottom electrode was suggested, a study of the cross-section of the PMNT600 sample became necessary. Figure 7a shows the corresponding TEM micrograph. The result coincides very well with the model presented in Fig. 4 for the columnar grown film. In fact, this result can explain why the Ru Auger signal is still present as the PMNT film is inspected, the reason being Ru diffusion through the voids between PMNT columns. An amorphous interfacial layer is also observed between the PMNT and TiN electrode, which could be evidence of a pyrochlore phase, as was pointed out by the XRD and AES results. On the other hand, Fig. 7b shows a TEM micrograph displaying the granular structure of the PMNT600 film, where the grains are surrounded by voids. In spite of the poor interface features and the presence of voids that permit Ru diffusion, a high degree of crystallization occurs at this temperature, as is shown in Fig. 7b by the large PMNT grains. A high-resolution micrograph of the grains is shown in Fig. 7c, where coupling between grains is observed, making evident the polycrystalline nature of the film.

Figure 8 shows the cross-section of the PMNT/TiN/SiO_2/Si film postannealed at 550°C. The columnar growth is maintained at this temperature. Focusing on the PMNT-TiN interface, an amorphous interfacial layer was not detected. The growth of a continuous PMNT layer on the TiN is initially observed followed by columnar growth until the final thickness is reached. This growth process will have an important effect on the dielectric properties of the PMNT film [29].

Lead deficient pyrochlore grains, whose structure is isostructural with that of $Pb_2Nb_2O_7$-type pyrochlore, were observed at the PMNT-TiN interface. A pyrochlore grain is shown in Fig. 9a, with planes (400) and (040) along the [001]

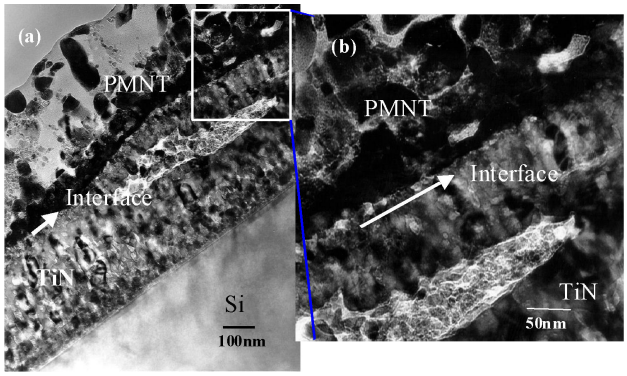

FIGURE 8. Cross-section TEM micrograph of the PMNT/TiN:O_2/Si ferroelectric thin film postannealed at 550°C (PMNT550), where no amorphous interfacial layer in the PMNT-TiN interface is observed.

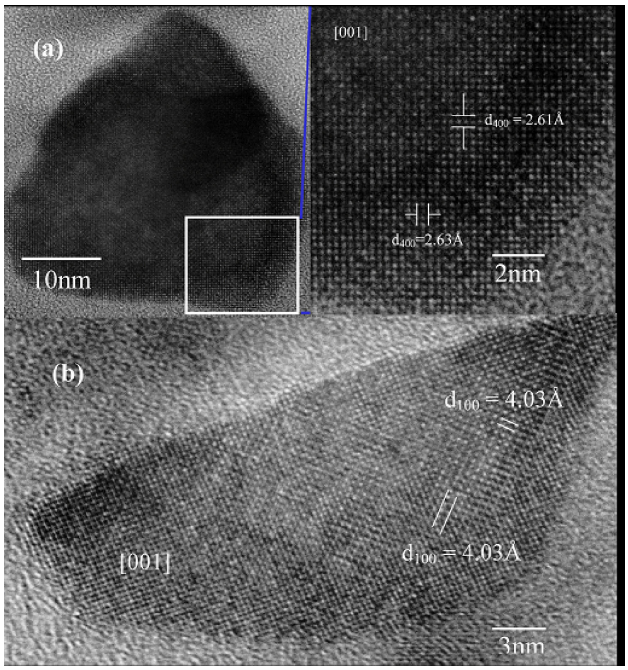

FIGURE 9. High resolution TEM micrograph of a) a pyrochlore grain observed in the PMNT550 sample, where the (400) and (040) planes in the [100] zonal axis are observed, and b) a perovskite grain with the (100) and (010) planes observed along the [100] zonal axis.

zone axis, where the interplanar spacings are d_{400}=2.61Å and d_{040}=2.63Å. The presence of the pyrochlore phase is to blame for the ferroelectric fatigue observed in PMNT films under a dc field and UV radiation (λ = 356nm) [29]. On the other hand, Fig. 9b shows a grain with a perovskite structure, where planes (100) and (010) are observed along the [001] zone axis with interplanar spacing d_{100}= 4.03Å.

The main difference in the microstructure of the films deposited at 500 and 600°C is found in the peculiarities of the respective interfaces that eventually will have an influence on the electric properties as previously reported [29]. Even though crystalline PMNT was obtained at lower temperatures than it is by most authors, it is clear that more work must be done to control composition, phase purity and interface properties and to assess the viability of TiN as electrode material. Lead deficiency and pyrochlore formation may be addressed by better controlling the deposition rate by optimizing the laser repetition rate and the oxidizing atmosphere to reduce lead loss. The electric properties may be improved by performing a Rapid Thermal Annealing on the films deposited at relatively low temperatures, of the order of 550°C for better crystallization.

4. Conclusions

$Pb(Mg_{1/3}Nb_{2/3})_{0.9}Ti_{0.1}O_3$ on TiN thin films was obtained by pulsed laser ablation and post annealed at 500, 550 and 600°C. XRD analyses showed the film annealed at 500°C consisted of a pure perovskite phase in contrast with those annealed at 550 and 600°C, which showed a dominant perovskite phase coexisting with a secondary pyrochlore phase that became more abundant as the annealing temperature was increased beyond 500°C. This behavior was explained by the high volatility of lead that produces an increasingly Pb^{2+} deficient solid solution as the temperature is increased, giving rise to the pyrochlore phase. As a result of the experimental process reported in this work, polycrystalline perovskite PMNT films were deposited on TiN electrodes at a lower temperature than those reported in the literature using other deposition techniques. Cracking of the films was observed in all cases after the annealing process, possibly due to the difference in thermal expansion coefficients of the PMNT and the substrate, suggesting heat treatments at lower temperatures. From the Auger and XPS spectra, it is concluded that TiN used as the bottom electrode is oxygenated to form $TiN:O_2$. This result seems to influence the growth habit of the PMNT film as observed in the TEM micrographs, where no amorphous layer is observed between the ferroelectric film and the electrode. TEM measurements support the columnar growth model suggested by (AES) measurements. No electrical short circuits between top and bottom electrodes were observed. Also, from TEM measurements, grains with perovskite and pyrochlore phases were shown. The pyrochlore grains were mainly located at the PMNT film-electrode interface, where an excess of Nb was detected by (AES), the excess of Nb being the main factor responsible for the formation of pyrochlore.

Acknowledgments

The technical support by I. Gradilla, E. Aparicio, and F. Ruiz is acknowledged. This work has been partially supported by CoNaCyT-México, through grant No. 47714-F and by DGAPA-UNAM grant No. IN102908.

1. X.Y. Zhao, B.J. Fang, H. Cao, Y.P. Guo, and H.S. Luo, *Mater. Sci. Eng. B* **96** (2002) 254.

2. Z.G. Ye, M. Dong, and Y. Yamashita, *J. Cryst. Growth* **211** (2000) 247.

3. J.H. Park, J. Park, J.G. Park, B.K. Kim, and Y. Kim, *J. Eur. Ceram. Soc.* **21** (2001) 1383.

4. F.F. Lorraine and D.A. Payne, *Mat. Res. Soc. Symp. Procc.* **200** (1990) 173.

5. S.L. Schwartz, T.R. Shrout, W.A. Schultz, and L.E. Cross, *J. Am. Cer. Soc.* **67** (1984) 311.

6. R.E. Cohen, *Nature, News and Views, Material Science* **441** (2006) 941.

7. Z. Kutnjak, J. Petzelt, and R. Blinc, *Nature, Letters* **441** (2006) 956.
8. N.J. Donnelly, G. Catalan, C. Morros, R.M. Bowman, and J.M. Gregg, *J. Appl. Phys.* **93** (2003) 9924.
9. J.P. Maria, W. Hackenberger, and S. Trolier-McKinstry, *Mat. Res. Soc. Symp. Procc.* **493** (1998) 421.
10. V. Nagarajan *et al.*, *Mat. Res. Soc. Symp. Procc.* **596** (2000) 505.
11. N.J. Donnelly, G. Catalan, C. Morros, R.M. Bowman, and J.M. Gregg, *Mat. Res. Soc. Symp. Procc.* **688** (2002) 337.
12. N.J. Donnelly, G. Catalan, C. Morros, R.M. Bowman, and J.M. Gregg, *Mat. Res. Soc. Symp. Procc.* **748** (2003) 367.
13. J.H. Park, F. Xu, and S. Trolier-Mckinstry, *J. Appl. Phys* **89** (2001) 568.
14. Z. Zhang, J.H. Park, and S. Trolier-McKinstry, *Mat. Res. Soc. Symp. Procc.* **596** (2000) 73.
15. A.Y. Liu *et al.*, *App. Phys. Lett.* **87** (2005) 72903.
16. S. Jaydeep, S. Yadav, B.P. Malla, and A.R. Kulkarnj, *Appl. Phys. Lett.* **81** (2002) 3840.
17. J.P. Maria, W. Hackenberger, and S. Trolier-McKinstry, *J. Appl. Phys.* **84** (1998) 5147.
18. T.H. Teng *et al.*, *Mat. Res. Soc. Symp. Procc.* **596** (2000) 37.
19. C.A. Randall and A.S. Bhalla, *J. Matter. Sci.* **29** (1990) 5.
20. J. Chen, H.M. Chan, and M.P. Harmer, *J. Am. Ceram. Soc.* **72** (1989) 593.
21. P.Y. Jouan, M.C. Peignon, Ch. Cardinaud, and G. Lempériere, *Appl. Surf. Sci.* **68** (1993) 559.
22. M.H. Yeh, K.S. Liu, and I.N. Lin, *J. Mater. Res.* **9** (1994) 2379.
23. J. Chen, Q. Zhang, and L.E. Cross, *Mater. Res. Soc. Symp. Proc.* **310** (1993) 47.
24. N. Wakiya, A. Saiki, N. Ishizawa, and N. Mizutane, *Mater. Res. Bull.* **28** (1993) 137.
25. J. Chen and M.P. Harmer, *J. Am. Ceram. Soc.* **73** (1990) 68.
26. M. Kazemeini, A. Berezin, and N. Fukuhara, *Thin Solid Films* **372** (2000) 70.
27. K. Okuwada, M. Iami, and K. Kakumo, *Jpn. J. Appl. Phys.* **28** (1989) L1271.
28. Landolt-Börnstein 1981in *Numerical Data and Functional Relationships in Science and Technology, New Series, Ferroelectric and Related Substances, Subcolume a: Oxides* (Springer-Verlag, Heidelberg, New York).
29. A. Fundora and J.M. Siqueiros, *Thin Solid Films* **373** (2000) 60.
30. W.L. Warren, D. Dimos, and R.M. Waser, *Mater. Res. Bull.* **31** (1996) 40.